Atmospheric
Chemistry
and Physics
Discussions

Open Access

EGU

Photochemical age of air pollutants and oxidation products in transboundary air observed on Fukue Island, Nagasaki, Japan

S. Irei[1,a], A. Takami[1], Y. Sadanaga[2], S. Nozoe[1,b], S. Yonemura[3], H. Bandow[2], and Y. Yokouchi[1]

[1]National Institute for Environmental Studies, 16-2 Onogawa, Tsukuba, Ibaraki 305-8506, Japan
[2]Department of Applied Chemistry, Graduate School of Engineering, Osaka Prefecture University, 1-1 Gakuencho, Naka-ku, Sakai, Osaka 599-8531, Japan
[3]National Institute for Agro-Environmental Sciences, 3-1-3 Kannondai, Tsukuba, Irabaki 305-8604, Japan
[a]present address: Department of Biology, Chemistry, and Marine Science, University of the Ryukyus, 1 Senbaru, Nishihara, Okinawa 903-0213, Japan
[b]present address: National Museum of Emerging Science and Innovation, Aomi 2-3-6, Koto, Tokyo 135-0064, Japan

ACPD

doi:10.5194/acp-2015-840

Title Page

Abstract	Introduction
Conclusions	References
Tables	Figures

|◀ | ▶|

◀ | ▶

Back | Close

Full Screen / Esc

Printer-friendly Version

Interactive Discussion

Title Page

Abstract | Introduction

Conclusions | References

Tables | Figures

|◄ | ►|

◄ | ►

Back | Close

Full Screen / Esc

Printer-friendly Version

Interactive Discussion

Photochemical age and oxidation products in transboundary air, Japan

S. Irei et al.

Abstract

To better understand the secondary air pollution in transboundary air over western-most Japan, ground-based field measurements of the chemical composition of fine particulate matter ($\leq$ 1 μm), mixing ratios of trace gases species (CO, O_3, NO_x, NO_y, i-pentane, toluene, and ethyne), and meteorological elements were conducted with a suite of instrumentation. The CO mixing ratio dependence on wind direction showed that there was no notable influence from primary emission sources near the monitoring site, indicating long- and/or mid-range transport of the measured chemical species. Despite the considerably different atmospheric lifetimes of NO_y and CO, these mixing ratios were correlated (r^2 = 0.67), suggesting negligible loss of NO_y by the reaction with OH radical. The photochemical age of the pollutants, t[OH], was calculated from both the NO_x/NO_y concentration ratio (NO_x/NO_y clock) and the toluene/ethyne concentration ratio (hydrocarbon clock). It was found that the toluene/ethyne concentration ratio was significantly influenced by dilution with background air containing 0.16 ppbv of ethyne, causing significant bias in the estimation of t[OH]. In contrast, the influence of the reaction of NO_x with O_3, a potentially biasing reaction channel on $[NO_x]/[NO_y]$, was small. The t[OH] values obtained with the NO_x/NO_y clock were compared with the fractional contribution of the m/z 44 signal to the total signal in the organic aerosol mass spectra (f_{44}, a quantitative oxidation indicator of carboxylic acids), and the comparison showed evidence for a systematic increase of f_{44} as t[OH] increased. To a first approximation, the f_{44} increase rate was 1.05×10^{-9} h^{-1} molecule^{-1} cm^3, which is comparable to the background-corrected increase rate observed during the New England Air Quality Study in summer 2002.

1 Introduction

During the last decade, the dramatic growth of the Chinese economy has increased emission of air pollutants such as volatile organic compounds, particulate matter (PM),

and nitrogen oxides (NO_x), which is the sum of nitrogen monoxide (NO) and nitrogen dioxide (NO_2). In northeast Asia, air masses generally move from east to west, and therefore pollutants emitted on continental China are frequently carried to Japan. The influence of transboundary air pollution is becoming severe in rural areas of western-most Japan, such as Fukue Island. Atmospheric oxidation of primary pollutants produces secondary pollutants, such as ozone (O_3), secondary particulate organic matter (also known as secondary organic aerosol or SOA), which is formed by oxidation of volatile organic precursors. A better understanding of these secondary pollutants is important not only for purely scientific reasons but because such pollutants are a matter of great public concern. SOA is one of the least understood subjects in atmospheric chemistry (Ebben et al., 2014), despite the fact that it has been studied extensively owing to its potential adverse effects on human health and its role in cloud condensation. Although state-of-the-art techniques, such as aerosol mass spectrometry, have substantially improved our understanding of SOA (Zhang et al., 2005; Jimenez et al., 2009), many questions about SOA still remain, such as its constituents, production mechanisms, and fates.

To understand SOA, we must evaluate the progress of the chemical reactions of its constituents. The progress of photochemical reactions in the atmosphere has frequently been evaluated in terms of a "photochemical age," designated t[OH], which can be derived from non-methane hydrocarbon (NMHC) ratios (Roberts et al., 1984; Rudolph and Johnen, 1990) or from NO_x ratio to total odd nitrogen (NO_y) (Parrish et al., 1992). Recent field studies combining aerosol mass spectrometry measurements and determination of t[OH] have provided new information about photochemically produced SOA (de Gouw et al., 2005; Takegawa et al., 2006; Kleinman et al., 2007; Liggio et al., 2010). Our previous field studies conducted on Fukue Island in Japan demonstrated a strong association between particulate carboxylate concentrations and t[OH], evidence of SOA production (Irei et al., 2014). However, the study period was short (only 10 days), and a longer observation period is necessary to obtain more-convincing evidence of SOA production. Furthermore, inconsistent results regarding the association

between SOA production and t[OH] were observed at the same location during a different time period (Irei et al., 2015). The study described in this paper is an extension of our previous studies, and the objective was to deepen our understanding of the association between oxidation products (SOA and O_3) and t[OH] in transboundary air.

2   Experimental

Field measurements were conducted from December 2010 to May 2011 at the Fukue atmospheric monitoring station (32.8° N, 128.7° E), a rural site on the northwestern peninsula of Fukue Island, Nagasaki Prefecture, Japan (Fig. 1). As mentioned earlier, data collected at the same measurement site during a 10 day observation period in December 2010 have already been reported (Irei et al., 2014). The monitoring station is ∼ 1 km away from the residential area of the peninsula and is ∼ 60 m higher in altitude. Possible sources of anthropogenic emissions of fine aerosol and trace gas species include agricultural waste burning, home incinerators, and automobiles occasionally passing by the station. For all the measurements the ambient air was measured or sampled 1 ∼ 3 m above the rooftop of the station (3 ∼ 5 m height from the ground). An independent sampling line was assembled for each chemical species measurement. The ambient air was sampled at 1 L min^{-1} through 5 m × quarter-inch o.d. PTFE tubing for the CO and O_3 measurements and at 0.5 L min^{-1} through the same type of tubing for the NO_x and NO_y measurements, respectively. For the particle and NMHC measurements, the ambient air was suctioned at 3 and 5 L min^{-1} at the first stage through the sampling lines of ∼ 4 m × half-inch o.d. and ∼ 10 m × five-eighth-inch o.d. stainless steel tubing (GL Science, Japan), respectively. The measurements were then made by sampling a part of the flowing air. It should be noted that, for the particle measurements only, a $PM_{2.5}$ cyclone separator (URG 2000-30ED, URG Corp. Chapel Hill, NC, USA.) was attached to the inlet of the sampling line to cut off particles larger than $PM_{2.5}$.

The 10 min average chemical composition of fine aerosol (∼ $PM_{1.0}$) was measured with an Aerodyne quadrupole aerosol mass spectrometer (AMS, Aerodyne Research

Inc., Billerica, MA, USA). Details of the instrumentation and the method for determination of chemical species concentrations are described elsewhere (Jayne et al., 2000; Allan et al., 2004). The AMS was calibrated approximately once a month with 350 nm dried ammonium nitrate particles for determination of ionization efficiencies. The temperature of the flash vaporizer was set to 873 K during the field measurements and calibration measurements. A collection efficiency of 0.74 was used for determination of chemical species concentrations; this value was determined from comparison between sulfate concentrations measured by means of AMS and non-sea-salt sulfate concentrations determined by means of total suspended particulate filter sample analysis during the field study in December 2010 (Irei et al., 2014). The detection limits (DLs) of the mass spectrometer for chloride, nitrate, ammonium, sulfate, organics, m/z 43 (an indicator for detection of hydrocarbon and aldehyde), and m/z 44 (an indicator for detection of carboxylic acid) were determined by 3× standard deviation (SD) of blank concentrations obtained by measuring filtered ambient air (HEPA Capsule, Pall Corp.) for 2 ~ 16 h. The blank measurements were conducted every month during the study period. The average DLs of these species were 0.02, 0.04, 0.2, 0.4, 0.5, 0.02, and 0.06 $\mu g\,m^{-3}$, respectively.

Mixing ratios for NO_x and NO_y were measured in situ to retrieve the t[OH], an indicator of atmospheric oxidation. NO_x and NO_y analyzers with an LED converter and a molybdenum converter, respectively, were developed from commercially available NO_x analyzers (Model 42 i-TL, Thermo Scientific). These instruments are described in detail elsewhere (Sadanaga et al., 2010; Yuba et al., 2010). DLs for both instruments were about 0.06 ppbv. Mixing ratios of CO and O_3 were measured in situ with a CO analyzer (Model 48, Thermo Scientific) and an O_3 analyzer (Model 49i, Thermo Scientific), respectively. The DLs of these instruments were 10 and 5 ppbv, respectively. The analog signal output for these trace gas species was recorded every second using a data logger (NR-1000, KEYENCE), and hourly average mixing ratios were used for data analysis. Selected NMHCs (ethyne, i-pentane, and toluene) were also measured hourly with a gas chromatograph equipped with a flame ionization detector (6890N,

Agilent Technologies) and coupled with an automated cryo preconcentration sampler (Yokouchi, 2008). Ethyne, *i*-pentane, and toluene were chosen because those can be used as markers for vehicular emissions (Tang et al., 2009; Wang et al., 2015). The choice of toluene was also owing to one of the possible precursors of atmospheric SOA (Grosjean and Seinfeld, 1989; Seinfeld and Pandis, 1999). The volatile organic compounds in 600 mL of ambient air were collected cryogenically from the main stream of the previously referred sampling line at a flow rate of 40 mL min^{-1} (i.e., a 15 min sampling period for a single measurement). Target compounds were identified and quantified on the basis of comparison with retention times and peak area counts for standards; specifically, a standard gas containing 1 ppb of each target compound was analyzed once a day. The DLs for ethyne, *i*-pentane, and toluene were 2,5, 1.5, and 1.5 parts per trillion, respectively.

Additionally, ambient temperature, relative humidity (RH), precipitation, and wind speed and direction were measured with a weather transmitter (WXT 520, VAISALA, Helsinki, Finland).

3   Results and discussion

3.1   Meteorological observations

Measured ambient temperature ranged from −1.5 to 25.1 °C (mean ± standard deviation or SD = 10.5 ± 5.4 °C). The temporal variations of observed hourly average ambient temperature, RH, and precipitation are shown in Fig. S1 in the Supplement. Ambient temperature showed clear seasonal variation, and a polynomial best fit curve ±5 °C covered ∼ 90 % of the data points and reproduced the observed trend.

Precipitation events were observed occasionally, but their frequency and strength did not seem to significantly affect our interpretation of the entire data set. Therefore, in the analyses described hereafter, we included the data collected during the precipitation events, unless otherwise noted. RH varied between 25 and 100 % and seemed to be

relatively constant from December to February and to vary more widely from March to May.

A polar plot of hourly average wind speed shows that it ranged from 0.2 to $10\,\mathrm{m\,s^{-1}}$ (Fig. S2 in the Supplement). The mean $\pm$ SD of wind speeds during the observation period was $3 \pm 1\,\mathrm{m\,s^{-1}}$, and the 90th, 25th, and 10th percentile cut-off values were 4, 2, and $1\,\mathrm{m\,s^{-1}}$, respectively. This information suggests that medium-strength winds (i.e., wind speeds of 2–$4\,\mathrm{m\,s^{-1}}$) blew most of the time during the study period. Because wind directions measured at wind speeds of $< 1\,\mathrm{m\,s^{-1}}$ are often treated as invalid, the fact that the 10th percentile cut-off for our data was $1\,\mathrm{m\,s^{-1}}$ indicates that 90 % of our wind direction data were valid. The most prevalent wind directions were between northwesterly and northeasterly (35 %) and between northeasterly and southeasterly (26 %). The prevalence of wind from the residential area of the peninsula (from the direction between southeasterly and southwesterly) was about 17 %.

3.2 Chemical species concentrations

The results of statistical analysis of the concentrations of chemical species in fine PM are summarized in Table 1, along with the results for gas-phase species. Note that because sea-salt PM tends to be coarse, the very low concentrations of chloride measured by means of AMS indicate that most of the chloride originating from sea salt was eliminated at the AMS inlet, which selects for fine PM. The mean concentrations ($\pm$SD) of the chemical species in fine PM were similar to those observed in 2003 at the same location (Takami et al., 2005) and at Cape Hedo, Okinawa (Takami et al., 2007). Sulfate was the predominant chemical species in fine PM throughout the observation period, accounting for 46 % on average, and was followed by organics (29 %), ammonium (16 %), and nitrate (8.0 %). Note that the concentrations of nitrate, the detection of which is often an indication of the proximity of its emission source, were high in this study even though the monitoring station was located in a rural area. In many cases, the amount of nitrate in fine PM decreases or shifts to larger PM during long-range transport (Takiguchi et al., 2008, and references therein). Because there are no large

emission sources of nitrate around the monitoring station, the high nitrate concentrations probably indicate mid-range transport of pollutants from locations off the island. Temporal variation of the concentrations of organics in fine PM measured by means of AMS showed no seasonal trend, but some high-concentration episodes were observed (Fig. 2). In a time-series plot of the fraction of m/z 44 in the organic mass spectrum (f_{44}), f_{44} seemed to rise from ~ 0.12 to ~ 0.15 around the end of March. This increase may have been due to greater production of oxygenated organic compounds in spring than in winter because of the increasing sunlight irradiance in the spring, which was indicated by the times-series plot of ambient temperature (Fig. S1). It should be noted that Fig. 2 also demonstrates that the concentrations of organic aerosols in the study period from 6 to 16 December, which was previously reported (Irei et al., 2014), were relatively low.

Most of the O_3 mixing ratios were < 55 ppbv, and the mean of 45 ppbv was consistent with the annual mean of ~ 50 ppbv observed at the same location in 2011 (Kanaya et al., 2015); this annual mean of ~ 50 ppbv was the lowest annual mean O_3 mixing ratio observed over the course of 6 years (2009–2014) at this location by Kanaya et al. A times-series plot of hourly average O_3 mixing ratios showed that although there were some episodes of high mixing ratios, the mixing ratios seemed to vary between ~ 25 and ~ 50 ppbv from December to February and then were prone to gradually increase from the beginning of March to May (Fig. 3a). Similar seasonal trends have been observed at the same location (Kanaya et al., 2015) and at other remote sites in East Asia (Pochanart et al., 2002; Suthawaree et al., 2008; Kanaya et al., 2015, references therein). This trend was similar to the f_{44} trend described above and therefore can also be explained in terms of an increase in sunlight irradiance of polluted air masses transported from the Asian continent. Meanwhile, according to the observations at the other remote sites referred above, the O_3 mixing ratios tend to drop starting in May and continuing into the summer because the origin of air masses changes from the continent directly to the Pacific Ocean; the oceanic air masses generally contain much lower quantities of O_3 and its precursors. The drop in the O_3 mixing ratios observed between

9 May and 12 May was compatible with the influence of the oceanic air masses demonstrated by the back trajectories of air masses (Fig. S3 in the Supplement) modeled by HYSPLIT (Draxler and Rolph, 2013).

The NO_x mixing ratios ranged from lower than the DL to 12.70 ppbv (mean $\pm$ SD = 1.39 $\pm$ 1.16 ppbv), and the NO_y mixing ratios ranged from 0.13 to 25.41 ppbv (mean $\pm$ SD = 4.86 $\pm$ 3.49 ppbv). The upper quartile cut-offs for these mixing ratios were 1.70 and 6.03 ppbv, respectively. Compared to the mixing ratios observed in other field studies (Pandey Deolal et al., 2012, and references therein), most of these mixing ratios fell between those observed at European rural and background sites. No time-dependent trend was observed for the NO_x or NO_y mixing ratio (Fig. 3b and c). Episodes of high mixing ratios were observed irregularly.

The CO mixing ratios ranged from 57 to 1136 ppbv, and the median, upper, and lower quartile cut-off values were 204, 272, and 160 ppbv, respectively; no seasonal trend was observed (Fig. 3d). Except for some episodes of high mixing ratios, the observed mixing ratios below the upper quartile cut-off seem to be comparable in magnitude to those observed from 2002 to 2005 at various rural and remote locations in the region of the East China Sea (Suthawaree et al., 2008; Tanimoto et al., 2008), indicating that the mixing ratios we observed reflected the background mixing ratios in this region. A polar plot of the wind-sector dependence of the CO mixing ratio showed almost no sharp increases attributable to local anthropogenic emissions (Fig. S4 in the Supplement). The episodes of high mixing ratios that occurred at irregular intervals were attributed to mid-range transport of anthropogenic emissions.

To determine whether these episodes were due to combustion-related pollution transported from the Asian continent, we chose seven time periods with high CO mixing ratios that lasted for more than 24 h, and we checked the back trajectories of the air masses modeled by HYSPLIT. These episodes are listed in Table S1 in the Supplement, together with qualitative observations about the concentrations of other chemical species during the high-CO episodes. Back trajectories for each episode showed that the air masses were transported from the Asian continent during these episodes and

Title Page

Abstract | Introduction

Conclusions | References

Tables | Figures

|◄ | ►|

◄ | ►

Back | Close

Full Screen / Esc

Printer-friendly Version

Interactive Discussion

that the episodes ended with the arrival of air masses from the Pacific Ocean or Mongolia (Figs. S5–S11 in the Supplement). Thus, these results support the proposition that at least these seven high-concentration episodes were derived from the Asian continent.

⁵ Most of the observed mixing ratios for i-pentane, toluene, and ethyne (Table 1) were slightly higher than the ratios observed at Cape Hedo, Okinawa, in 2000 (Kato et al., 2004). This result is consistent with the fact that pollutants transported from the Asian continent to Fukue are often fresher than those transported to Cape Hedo (Takami et al., 2007). Times-series plots of the mixing ratios for these NMHCs showed no sea-
¹⁰ sonal trends (Fig. 3e–g). Note that in terms of outliers, high mixing ratios of i-pentane, toluene, and ethyne – which lasted no more than a few hours, indicating the influence of anthropogenic emissions near the site – accounted for only a small portion of the observed data.

3.3 Correlations between the concentrations of various chemical species

¹⁵ Investigation of the correlations between the concentrations of various chemical species showed that CO concentration was highly correlated with the concentrations of NO_y ($r^2 = 0.674$), ethyne ($r^2 = 0.724$), and organic aerosols ($r^2 = 0.562$) (Table 2). Ethyne is often used as a vehicular emission marker, and vehicles are major sources of NO_y. The lifetimes of CO, ethyne, and NO_y with respect to reactions with OH
²⁰ radicals (the most powerful oxidant in the air) at an average OH concentration of 5×10^5 molecules cm^{-3}, are approximately 100, 26, and 1.7 days, respectively. Even though the lifetime of NO_y is considerably shorter than the lifetimes of CO and ethyne, the high correlations probably indicate that NO_y and CO were transported to the monitoring station over a short period, during which loss of NO_y due to reaction with OH
²⁵ radicals was negligible. The slope of the line derived by linear regression was approximately 0.03, which differs significantly from the value of ~ 0.1 observed in 2002 by Takegawa et al. (2004). However, the slope of 0.03 was close to that for an air mass transported a long distance from its origin found by Kim et al. (2012) in numerical stud-

11

ies using a recent emission inventory. Thus, the low slope of 0.03 was more likely due to the recently improved emission of NO_y.

Particulate ammonia was highly correlated with particulate acidic components, such as sulfate, nitrate, organics, and m/z 44 of organics. The high correlation with organics suggests that in major the organics composed of carboxylic acids. The observed high correlations imply that sufficient amount of ammonia was available in the gas-phase to neutralize all these acidic components. Although it is not shown, slopes of linear regressions between ammonia (x axis) and sulfate, nitrate, or organics (y axis) was 1.7, 0.74, and 1.0, respectively. With respect to molar ratio to ammonia, sulfate and nitrate accounted for 32 and 21 %, respectively. Given that all three acidic species are neutralized with ammonia, organics, molar mass of which is unknown, accounts for 16 %. This number in turn gives the average molecular weight of organics as 113 g mol^{-1} for monocarboxylate.

The overall correlation between m/z 43 and m/z 44 in the organic mass spectra obtained by AMS was 0.640, but a plot of m/z 43 vs. m/z 44 showed two distinct trends: a trend with an m/z 44 to m/z 43 ratio of ∼ 1 and another with a ratio of ∼ 2.5 (Fig. S12 in the Supplement). This result suggests that two types of organic species gave fragment ions that contributed to the m/z 44 to m/z 43 ratio. These species will be discussed in detail in Sect. 3.4.

3.4 Oxidation state of organic aerosols

As we did in previous reports for the field studies in December 2010 (Irei et al., 2014) and in March 2012 (Irei et al., 2015), here we briefly discuss the results of evaluation of the oxidation state of the organic aerosols observed during the half-year period of this study. First, we applied positive matrix factorization (PMF) analysis to the organic aerosol mass spectra to deconvolute the types of organic aerosols (Zhang et al., 2005; Ulbrich et al., 2009), and then we determined the oxidation state of each type of organic aerosol by plotting the fractions of m/z 43 (f_{43}) and m/z 44 (f_{44}) in the organic mass spectra, according to the method described by Ng et al. (2010). Furthermore, we

determined the mass to carbon ratios (OM/OC ratios) of the types of organic aerosol using the method described by Zhang et al. (2005) to characterize the species of the organic aerosols.

With respect to the mass spectral pattern, PMF analysis gave the most feasible solution with two types of organic aerosols: hydrocarbon-like organic aerosol (HOA) and low-volatility oxygenated organic aerosol (LV-OOA). The mass spectral patterns of these two types of aerosols (Fig. 4) agreed well with those of HOA and LV-OOA found in the December study. The patterns also agreed reasonably with the reference mass spectra for HOA and LV-OOA in the AMS spectral database made available by Ulbrich et al. (2009, http://cires.colorado.edu/jimenez-group/AMSsd/). The time-series variations of the HOA and LV-OOA mass concentrations showed similar patterns (Fig. 5). On average, HOA and LV-OOA accounted for 38 and 59 % of the organic aerosols throughout the study period, respectively. In a plot of f_{43} vs. f_{44}, that data point for LV-OOA in this study was located at the top of the triangle, indicating a high oxidation state (Fig. 6). The OM/OC ratio of HOA and LV-OOA were 2.8 and 5.0 $\mu g \, \mu g \, C^{-1}$, respectively. The OM/OC ratio of HOA was twice as high as the ratio of HOA found in the December study. This may be an implication of oxidation of HOA at some extent. The OM/OC ratio of LV-OOA was only 1.4 and 1.2 times as high as the ratios of LV-OOA found in our field studies in December 2010 and March 2012, respectively. To the best of our knowledge, substances showing such a high OM/OC ratio are only humic-like substances.

3.5 Chemical clocks

We used the NO_x/NO_y concentration ratio and a NMHC concentration ratio to explore the extent of chemical reactions. In this type of chemical clock analysis, the concentration of a reactive chemical and that of a less reactive chemical are used in the numerator and the denominator, respectively, of the ratio. As a reaction proceeds, the numerator decreases while the denominator remains constant; therefore, a change in the ratio indicates the extent of reaction. In application of chemical clocks to the atmo-

13

spheric transport of pollutants, it must be remembered that because, in many cases, emission sources are spatially distributed over the trajectory of an air parcel, the extent of reaction may not always be well defined. This type of analysis is ideally suited to situations in which inputs into an air parcel from additional emission sources during transport are negligible. Our field study for transboundary air pollution transported over the East China Sea can be the ideal case. To see if such an assumption is valid, the NO_x/NO_y and hydrocarbon clocks were evaluated.

Given that the conversion of NO_2 (the major component of NO_x) to HNO_3 (one of the components of NO_y)

$$NO_2 + OH \xrightarrow{M} HNO_3 \tag{R1}$$

is the major sink for NO_x and that the concentration of OH radicals, [OH], can be assumed to be constant, the photochemical age, t[OH], of NO_x can be determined according to the following pseudo-first order rate law:

$$t[OH] = -\frac{1}{k_{NO_2}} \ln \frac{[NO_x]}{[NO_y]} \tag{1}$$

where $[NO_x]$, $[NO_y]$, and k_{NO_2} are the concentrations of NO_x and NO_y (molecules cm^{-3}) at reaction time t and the temperature-dependent effective second-order rate constant for the reaction of NO_x with OH radicals, respectively. Note that k_{NO_2} includes the concentration of a third body, [M], which depends on pressure and temperature. To calculate k_{NO_2} at ambient temperature and a pressure of 1 atm, we therefore calculated the third-order rate constant and [M] according to the method described by Finlayson-Pitts and Pitts (2000) with the polynomial best fit for measured ambient temperature mentioned in Sect. 3.1. The calculated k_{NO_2} values at 1 atm ranged from 9.3×10^{-12} to 1.1×10^{-11} cm^3 molecule^{-1} s^{-1}, and both the mean and the median were 1.0×10^{-11} cm^3 molecule^{-1} s^{-1}. In turn, the determined t[OH] using the k_{NO_2} values and the $[NO_x]/[NO_y]$ ratios ranged from 2.9×10^5 to 1.3×10^8

(mean $\pm$ SD = $(3.4 \pm 1.6) \times 10^7$ h molecules cm^{-3}). We found that the use of a fixed k_{NO_2} value (i.e., the mean value of 1.0×10^{-11} cm^3 molecule^{-1} s^{-1}) resulted in biases between -10 and $+5$ % in the estimation of t[OH]. We also found that a temperature variation of ± 5 K resulted in only a ± 5 % variation in t[OH]. However, note that this analysis for the biases does not take into account temperature and pressure variations during the transport of the air parcels.

The reaction of NO$_2$ with O$_3$, which may result in significant overestimation in the NO$_x$/NO$_y$ clock, was also evaluated. The reaction of NO$_2$ with O$_3$ forms NO$_3$ radicals:

$$NO_2 + O_3 \longrightarrow NO_3 + O_2 \tag{R2}$$

This reaction channel is significant at night, but insignificant during the day when NO$_3$ radicals are quickly photolyzed back to NO$_x$. NO$_3$ radicals react with NO$_2$ to form stable N$_2$O$_5$, which is in thermal equilibrium with NO$_2$ and NO$_3$ and therefore acts as a reservoir of NO$_x$:

$$NO_2 + NO_3 \leftrightarrow N_2O_5 \tag{R3}$$

N$_2$O$_5$ reacts slowly with water vapor to form HNO$_3$, and this process terminates the chain reaction:

$$N_2O_5 + 2H_2O \longrightarrow 2HNO_3 \tag{R4}$$

The reaction of N$_2$O$_5$ with water vapor is a significant reaction channel when the RH is above 50 % (Finlayson-Pitts and Pitts, 2000, and references therein), which was the case in our study (Fig. S1). Thus, the contribution of the reaction of NO$_2$ with O$_3$ may result in a significant overestimation of t[OH].

We evaluated the significance of this reaction channel by comparing the lifetime of NO$_x$ with respect to reaction with OH radicals, τ_{OH}, and with respect to reaction with O$_3$, τ_{O_3}, at constant OH radical and O$_3$ concentrations. For this evaluation, we used $1.0 \times$

10^{-11} and 3.2×10^{-17} cm^3 molecule^{-1} s^{-1} at 298 K and 1 atm as the second-order rate constants for the two reactions, respectively, and 1×10^6 and 1.0×10^{12} molecules cm^{-3} (0.05 and 52 ppbv) as the OH and O_3 concentrations, respectively. The values of τ_{OH} and τ_{O_3} were calculated to be 27 and 6.8 h, respectively. That is, the loss of NO_x due to reaction with O_3 was approximately 4 times as fast as that due to reaction with OH radicals under these conditions. If the reaction of NO_2 with O_3 at night was the predominant mode of conversion of NO_x to NO_y, a positive correlation between the O_3 mixing ratio and the extent of NO_x turnover – that is, between the O_3 mixing ratio and $\ln([NO_x]/[NO_y])$ – should be observed. However, a plot of the O_3 mixing ratios vs. $\ln([NO_x]/[NO_y])$ showed an inverse correlation ($r^2 = 0.489$), indicating that the turnover of NO_x to NO_y increased as the O_3 mixing ratio increased (Fig. 7). Similar observations have been reported elsewhere (Olszyna et al., 1994; Roussel et al., 1996). Given that during the day, O_3 forms only photochemically, this inverse correlation suggests that NO_x conversion was due to daytime photochemistry. A conclusion with this possibility was drawn from an analysis of O_3 production efficiency (Yokouchi et al., 2011). For the OH radical reaction to be at least as significant as the O_3 reaction, [OH] through the study period would have to have been at least 3×10^6 molecules cm^{-3}, which is at least 6 times as high as the concentration reported previously (Irei et al., 2014). Previously reported concentrations of particulate chemical species were also substantially lower than the values here; therefore, the difference is consistent.

The photochemical reaction of aldehydes is also a sink for NO_2, resulting in the formation of thermally stable peroxyacyl nitrates:

$$RCHO + OH \longrightarrow RCO + H_2O \tag{R5}$$

$$RCO + O_2 \longrightarrow RC(O)OO \tag{R6}$$

$$RC(O)OO + NO_2 \longrightarrow RC(O)OONO_2 \tag{R7}$$

Unfortunately, we cannot evaluate the significance of this channel with our current dataset, because no data for aldehyde and peroxyacyl radical concentrations are available. Because this loss channel also occurs in sunlight, the possibility that peroxyacyl

16

Title Page

Abstract | Introduction

Conclusions | References

Tables | Figures

|◄ | ►|

◄ | ►

Back | Close

Full Screen / Esc

Printer-friendly Version

Interactive Discussion

nitrate formation significantly affects t[OH] cannot be excluded. The absolute value of t[OH] derived from the [NO_x]/[NO_y] ratio remains uncertain, but as demonstrated by the correlation between this ratio and the O_3 mixing ratio (r^2 = 0.489, Fig. 7), the use of the NO_x/NO_y clock nevertheless provides valuable information about the relative extent of photooxidation. When we plotted the time-series variation of t[OH] estimated from the [NO_x]/[NO_y] ratio (Fig. 8), we observed variation similar to that observed for the hourly average O_3 mixing ratio (Fig. 3a), implying a strong association between the t[OH] and the sunlight irradiance.

When NMHC A and B react with OH radicals at different rate

$$A + OH \longrightarrow Product + H_2O \tag{R8}$$

$$B + OH \longrightarrow Product + H_2O \tag{R9}$$

t[OH] can also be estimated from the ratio of the two NMHCs (Robert et al., 1984; Rudolph and Johnen, 1990; Parrish et al., 1992):

$$t[OH] = \frac{1}{(k_A - k_B)} \ln \left(\frac{[A_0]}{[B_0]} \cdot \frac{[B]}{[A]} \right) \tag{2}$$

where [A_0] and [B_0] are the initial concentrations (molecules cm^{-3}) of NMHCs A and B, which have short and long lifetimes (relative to each other); [A] and [B] are the concentrations (molecules cm^{-3}) at time t; and k_A, and k_B are the temperature-dependent second-order rate constants for reactions of A and B with OH radicals (molecule s^{-1} cm^3 s^{-1}). If NMHCs A and B are emitted from the same source at the same time, the change in the concentration ratio theoretically indicates the extent of chemical reaction. However, dilution with an aged air mass containing depleted NMHCs can also change the NMHC ratio, thus biasing the t[OH] estimation (McKeen and Liu, 1993). This bias can be visualized by plotting two different NMHC ratios with the same denominator. For this study, we plotted the natural logarithm of the [i-pentane]/[ethyne] ratio against the natural logarithm of the [toluene]/[ethyne] ratio (Fig. 9). Note that the calculations necessary for this plot require the rate constants

for the reactions of the NMHCs with OH radicals, the mixing ratios of the NMHCs in the background air, and their initial mixing ratios at emission. Using the Arrhenius equation with the recommended parameters for i-pentane, toluene, and ethyne (NIST Chemistry WebBook, http://webbook.nist.gov/chemistry/), respectively, the rate constants for the reaction of these compounds with OH radicals at 283 K (i.e., the mean temperature during the study period) were calculated to be 3.44×10^{-12}, 5.88×10^{-12}, and 7.38×10^{-13} cm^3 molecule^{-1} s^{-1}, respectively. For the background mixing ratios, we used mixing ratios observed at Cape Hedo, Okinawa (Kato et al., 2004), which were 0.05, 0.09, and 0.39 ppbv, respectively. For the initial mixing ratios at emission, we used the reported scores for loadings extracted by means of PMF analysis for volatile organic compound sources in Beijing (Wang et al., 2015). The extracted loadings reported were vehicular emissions 1 and 2, solvent use, and natural gas and gasoline leakage. In addition to these initial mixing ratios, mixing ratios reported a rural site in northeast China (Lin'an, in the Yangtze River Delta, Tang et al., 2009) were also tested.

The plot shows that, with respect to the initial NMHC ratio, depletion trends resulting from use of the solvent-use profile and of the observations in Lin'an deviated substantially from the observed overall trend (Fig. 9). The observed trend lies between the trends for the dilution with the background air and the reaction loss calculated using the vehicular-emissions profiles and the natural-gas and gasoline leakage profile. Note that the reaction loss was calculated based on the mean temperature observed, 10.5 °C. The variation of the slope for the reaction loss owing to the variation of the temperature-dependent rate constants between the maximum and minimum temperature (25.1 and −1.5 °C) was found to be less than ±2 %. Thus, the variation of the reactive loss due to the temperature change was not influential to our analysis. The vehicular emissions and the natural gas and gasoline leakage may have been the predominant emitters of these NMHCs, but source apportionment is difficult because of the uncertainty in the emission profiles. On the basis of this comparison, we could identify only two possible significant sources of these NMHCs during the measurement period. A quantitative understanding will require a more sophisticated analysis

based on mass balance with reliable source profiles. Compared to the background mixing ratios observed at Cape Hedo, our observations were lower. This result implies that the background NMHC ratios from the observations at Cape Hedo are still too high to be used as background values for our calculation. With consideration of their life times (2, 3, and 16 days for toluene, i-pentane, and ethyne, respectively, under the [OH] of 1×10^6 molecules cm^{-3}), it is reasonable to assume that the background mixing ratios for both toluene and i-pentane in the aged air masses were below the DL (< 3 pptv). This assumption allows us to determine the background mixing ratio of ethyne when comparing with the smallest [toluene]/[ethyne] and [i-pentane]/[ethyne] ratios observed. According to Fig. 9, the background NMHC ratios seem to lie between -3.5 and -4. If we use the highest DL value (3 pptv) as the background mixing ratio for toluene and i-pentane, the background ethyne mixing ratio is then calculated to be ~ 0.16 ppbv, which is about 25 % of the background value observed at Cape Hedo by Kato et al. (2004). On the basis of the plot in Fig. 9, we recommend the use of 0.003, 0.003, and 0.16 ppbv as the background mixing ratios for i-pentane, toluene, and ethyne, respectively, in the region of the East China Sea.

3.6 Dependence of f_{44} on t[OH]

A scatter plot of f_{44} as a function of t[OH] estimated by the NO$_x$/NO$_y$ clock showed a proportional increase of f_{44} with increasing t[OH] (estimated by means of the NO$_x$/NO$_y$ clock) up to a t[OH] value of 7×10^7 h molecules cm^{-3}, and then f_{44} started to level off slightly (Fig. 10). That is, f_{44} works as an oxidation indicator below the t[OH] of 7×10^7 h molecules cm^{-3}. The f_{44} oxidation indicator is known to be case dependent, even at this location and below this upper limit (Irei et al., 2015). Considering the existence of HOA during the study period, a series of findings here and in the previous reports supports our hypothesis that f_{44} varies with t[OH] as LV-OOA, which has a constant value of f_{44}, mixes with the background-level HOA, which has a significantly lower constant value of f_{44} than LV-OOA (Irei et al., 2014). To a first approximation of

the increasing trend, f_{44} is given by

$$f_{44} = (1.05 \pm 0.03) \times 10^{-9} t[\text{OH}] + 0.103 \pm 0.001 \tag{3}$$

with an r^2 value of 0.369. The first approximation satisfactorily describes the increasing trend below a $t[\text{OH}]$ value of 7×10^7 h molecules cm^{-3}. The intercept of the first approximation indicates the f_{44} value for organic aerosol at a photochemical age of zero, that is, f_{44} at emission. The slope, which was 1.05×10^{-9} h^{-1} molecule^{-1} cm^3, indicates the rate of increase of f_{44}. Kleinman et al. (2007) observed that during the New England Air Quality Study, the background-corrected f_{44} value increased from 0.08 to 0.13 as $-\ln([\text{NO}_x]/[\text{NO}_y])$ increased from 0.1 to 1.3, which corresponds to an increase of $t[\text{OH}]$ from 3.2×10^6 to 42×10^6 h molecule cm^{-3}. These values give an increase rate of 1.3×10^{-9} h^{-1} molecule^{-1} cm^3, which is almost identical to the rate we calculated in this study. The overall proportionality of f_{44} with $t[\text{OH}]$ suggests that, like the NO_x/NO_y clock, f_{44} worked as an oxidation indicator during this study period. This, however, is inconsistent with our another report, in which no proportional increase of f_{44} was observed during the study in different year at the same location (Irei et al., 2015). Interestingly, our hypothesis of binary mixture of organic aerosol is still consistent with these contradicting cases.

It has been proposed that the increasing trend of f_{44} can be explained by a binary mixture of variable amount of LV-OOA depending on extent of reaction processing x and constant amount of HOA (Irei et al., 2014, Supporting Information):

$$f_{44} = \frac{{}^{\text{HOA}}f_{44} \cdot a \cdot \left(\frac{\text{OM}}{\text{OC}}\right)_{\text{HOA}} + {}^{\text{LVOOA}}f_{44} \cdot \left[0.3x \cdot b \cdot \left(\frac{\text{OM}}{\text{OC}}\right)_{\text{LVOOA}}\right]}{a \cdot \left(\frac{\text{OM}}{\text{OC}}\right)_{\text{HOA}} + \left[0.3x \cdot b \cdot \left(\frac{\text{OM}}{\text{OC}}\right)_{\text{LVOOA}}\right]} \tag{4}$$

In this equation ${}^{\text{HOA}}f_{44}$ and ${}^{\text{LV-OOA}}f_{44}$ are the fractions of m/z 44 signal for the HOA and LV-OOA factors from the PMF analysis previously discussed, respectively;

20

$(OM/OC)_{HOA}$ and $(OM/OC)_{LV-OOA}$ are the organic mass concentration ratios to the organic carbon concentrations ($\mu g \, \mu g \, C^{-1}$) for the HOA and LV-OOA from the PMF analysis, respectively; and a and b values are arbitrary constants ($\mu g \, C \, m^{-3}$) that convert the $(OM/OC)_{HOA}$ and $(OM/OC)_{LV-OOA}$ ratios to the organic mass concentrations of the HOA and the LV-OOA, respectively. The factor "0.3", which is multiplied by the variable x, is a factor for the SOA carbon yield based on the laboratory experiments of SOA formation by photooxidation toluene (Irei et al., 2006, 2011). The Eq. (4) has one variable, x, and 6 parameters, the four of which are determined by PMF analysis. More progress in the extent of reaction processing, more contribution of LV-OOA to the binary mixture of HOA and LV-OOA, each of which has significantly different f_{44} value. Consequently, the f_{44} of the binary mixture containing a significantly low f_{44} continues to increase until it is saturated with LV-OOA. This hypothesis consistently explain our observations that the f_{44} oxidation indicator sometimes worked, and sometimes did not.

The f_{44} curve of organic aerosols was calculated using three different combinations of parameters listed in Table 3, (Fig. 11). It was found that the model calculation underestimated the f_{44} when 0.05 and $1 \, \mu g \, C \, m^{-3}$ were used for the a and b values, respectively, together with the rest of the parameters obtained from the PMF analysis (i.e., applying the parameters in the combination I in Table 3). Although these a and b values were used in the previous report and demonstrated reasonable agreement with the observations (i.e., applying the parameters in the combination III), the agreement was owing to different f_{44} values and OM/OC ratios extracted from the PMF analysis (see the Sect. 3.4). To have reasonable agreement with the observations using the f_{44} and OM/OC extracted by the PMF analysis, the use of 0.0175 and $1 \, \mu g \, C \, m^{-3}$ for the a and b values (applying the parameters in the combination II) was found to give the best fitting to the observations.

4 Summary

To improve our understanding of the oxidation products of atmospheric pollutants, we conducted field studies from December 2010 to May 2011 on Fukue Island, Nagasaki Prefecture, Japan. Wind-sector analysis of CO mixing ratios revealed that the ratio showed almost no wind-sector dependence, suggesting that the influence of emissions from residential areas near the measurement site was negligible. This fact in turn indicates that the influence of mid- and/or long-range transport of air pollutants to the site had a significant influence. Photochemical age, t[OH], was estimated from [NO_x]/[NO_y] and a NMHC concentration ratio, and the validity of the ratios was evaluated. The evaluation suggested that the hydrocarbon clock was significantly influenced by mixing with background air containing 0.16 ppbv of ethyne, a NMHC with a relatively long lifetime, resulting in significant bias in the estimation of t[OH]. In contrast, loss of NO_x due to reaction with O_3 at night did not seem to influence the NO_x/NO_y clock, which thus seemed to function appropriately. The t[OH] value obtained with the NO_x/NO_y clock was then compared with f_{44} obtained by AMS measurements, and f_{44} was observed to increase with increasing t[OH], indicating the f_{44} can be used as an oxidation indicator. This indicator likely works under the condition where two different types of organic aerosols, such as primary and secondary organic aerosols represented by hydrocarbon-like organic aerosols and low-volatile oxygenated organic aerosol, respectively, are mixed. Using linear regression analysis, we estimated that the f_{44} increase rate for organic aerosols transported over the East China Sea averaged 1.05×10^{-9} h^{-1} molecule^{-1} cm^3. This rate was almost identical to the background-corrected rate observed during the New England Air Quality Study in the summer of 2002.

Author contributions. Satoshi Irei contributed to the AMS, O_3, and meteorological measurements and is the person in charge of the data analysis and writing the manuscript. Akinori Takami is the person in charge of the AMS, O_3, and meteorological measurements. Yasuhiro Sadanaga is the person in charge of the NO_x and NO_y measurements. Seiichiro Yonemura is the person in charge of the CO measurements. Yoko Yokouchi is the person in charge of

the NMHC measurements. Susumu Nozoe contributed to the NMHC measurements. Hiroshi Bandow contributed to the NO_x and NO_y measurements.

References

Allan, J. D., Delia, A. E., Coe, H., Bower, K. N., Alfarra, M. R., Jimenez, J. L., Middlebrook, A. M., Drewnick, F., Onasch, T. B., Canagaratna, M. R., Jayne, J. T., and Worsnop, D. R.: A generalized method for the extraction of chemically resolved mass spectra from Aerodyne aerosol mass spectrometer data, J. Aerosol Sci., 35, 909–922, 2004.

de Gouw, J. A., Middlebrook, A. M., Warneke, C., Goldan, P. D., Kuster, W. C., Roberts, J. M., Fehsenfeld, F. C., Worsnop, D. R., Canagaratna, M. R., Pszenny, A. A. P., Keene, W. C., Marchewka, M., Bertman, S. B., and Bates, T. S.: Budget of organic carbon in a polluted atmosphere: results from the New England Air Quality Study in 2002, J. Geophys. Res.-Atmos., 110, D16305, doi:10.1029/2004JD005623, 2005.

Draxler, R. R. and Rolph, G. D.: HYSPLIT (Hybrid Single-Particle Lagrangian Integrated Trajectory) Model Access via NOAA ARL READY, NOAA Air Resources Laboratory, College Park, MD, available at: http://www.arl.noaa.gov/HYSPLIT.php (last access: 4 October 2015), 2013.

Ebben, C. J., Strick, B. F., Upshur, M. A., Chase, H. M., Achtyl, J. L., Thomson, R. J., and Geiger, F. M.: Towards the identification of molecular constituents associated with the surfaces of isoprene-derived secondary organic aerosol (SOA) particles, Atmos. Chem. Phys., 14, 2303–2314, doi:10.5194/acp-14-2303-2014, 2014.

Finlayson-Pitts, B. J. and Pitts Jr., J. N.: Chemistry of the Upper and Lower Atmosphere, Academic Press, San Diego, California, USA, 2000.

Grosjean, D. and Seinfeld, J. H.: Parameterization of the formation potential of secondary organic aerosols, Atmos. Environ., 23, 1733–1747, 1989.

Irei, S., Huang, L., Collin, F., Zhang, W., Hastie, D., and Rudolph, J.: Flow reactor studies of the stable carbon isotope composition of secondary particulate organic matter generated by OH-radical induced reaction of toluene, Atmos. Environ., 40, 5858–5867, 2006

Irei, S., Rudolph, J., Huang, L., Auld, J., and Hastie, D.: Stable carbon isotope ratio of secondary particulate organic matter formed by photooxidation of toluene in indoor smog chamber, Atmos. Environ., 45, 856–862, 2011.

Irei, S., Takami, A., Hayashi, M., Sadanaga, Y., Hara, K., Kaneyasu, N., Sato, K., Arakaki, T., Hatakeyama, S., Bandow, H., Hikida, T., and Shimono, A.: Transboundary secondary organic aerosol in western Japan indicated by the δ^{13}C of water-soluble organic carbon and the m/z 44 signal in organic aerosol mass spectra, Environ. Sci. Technol., 48, 6273–6281, 2014.

Irei, S., Takami, A., Sadanaga, Y., Miyoshi, T., Arakaki, T., Sato, K., Kaneyasu, N., Bandow, H., and Hatakeyama, S.: Transboundary secondary organic aerosol in western Japan: an observed limitation of the f_{44} oxidation indicator, Atmos. Environ., 120, 71–75, 2015.

Jayne, J. T., Leard, D. C., Zhang, X., Davidovits, P., Smith, K. A., Kolb, C. E., and Worsnop, D. R.: Development of an aerosol mass spectrometer for size and composition analysis of submicron particles, Aerosol Sci. Tech., 33, 49–70, 2000.

Jimenez, J. L., Canagaratna, M. R., Donahue, N. M., Prevot, A. S. H., Zhang, Q., Kroll, J. H., DeCarlo, P. F., Allan, J. D., Coe, H., Ng, N. L., Aiken, A. C., Docherty, K. D., Ulbrich, I. M., Grieshop, A. P., Robinson, A. L., Duplissy, J., Smith, J. D., Wilson, K. R., Lanz, V. A., Hueglin, C., Sun, Y. L., Laaksonen, A., Raatikainen, T., Rautiainen, J., Vaattovaara, P., Ehn, M., Kulmala1, M., Tomlinson, J. M., Collins, D. R., Cubison, M. J., Dunlea, E. J., Huffman, J. A., Onasch, T. B., Alfarra, M. R., Williams, P. I., Bower, K., Kondo, Y., Schneider, J., Drewnick, F., Borrmann, S., Weimer, S., Demerjian, K., Salcedo, D., Cottrell, L., Griffin, R., Takami, A., Miyoshi, T., Hatakeyama, S., Shimono, A., Sun, J. Y., Zhang, Y. M., Dzepina, K., Kimmel, J. R., Sueper, D., Jayne, J. T., Herndon, S. C., Trimborn, A. M., Williams, L. R., Wood, E. C., Kolb, C. E., Baltensperger, U., and Worsnop, D. R.: Evolution of organic aerosols in the atmosphere, Science, 326, 1525–1529, 2009.

Kanaya, Y., Tanimoto, H., Yokouchi, Y., Taketani, F., Komazaki, Y., Irie, H., Takashima, H., Pan, X., Nozoe, S., and Inomata, S.: Diagnosis of photochemical ozone production rates and limiting factors in continental outflow air masses reaching Fukue Island, Japan: ozone-control implications, Aerosol Air Qual. Res., in press, 2015.

Kato, S., Kajii, Y., Itokazu, R., Hirokawa, J., Koda, S., and Kinjo, Y.: Transport of atmospheric carbon monoxide, ozone, and hydrocarbons from Chinese coast to Okinawa Island in the western Pacific during winter, Atmos. Environ., 38, 2975–2981, 2004.

Kim, C.-H., Park, S.-Y., Kim, Y.-J., Chang, L.-S., Song, S.-K., Moon, Y.-S., and Song, C.-K.: A numerical study on indicators of long-range transport potential for anthropogenic particulate matters over northeast Asia, Atmos. Environ., 58, 35–44, 2012.

Kleinman, L. I., Daum, P. H., Lee, Y.-N., Senum, G. I., Springston, S. R., Wang, J., Berkowitz, C., Hubbe, J., Zaveri, R. A., Brechtel, F. J., Jayne, J., Onasch, T. B., and Worsnop, D.: Aircraft observations of aerosol composition and ageing in New England and Mid-Atlantic States during the summer 2002 New England Air Quality Study field campaign, J. Geophys. Res.-Atmos., 112, D09310, doi:10.1029/2006JD007786, 2007.

Liggio, J., Li, S.-M., Vlasenko, A., Sjostedt, S., Chang, R., Shantz, N., Abbatt, J., Slowik, J. G., Bottenheim, J. W., Brickell, P. C., Strond, C., and Leaitch, R. W.: Primary and secondary organic aerosols in urban air masses intercepted at a rural site, J. Geophys. Res.-Atmos., 115, D21305, doi:10.1029/2010JD014426, 2010.

McKeen, S. A. and Liu, S. C.: Hydrocarbon ratios and photochemical history of air masses, Geophys. Res. Lett., 20, 2363–2366, 1993.

Ng, N. L., Canagaratna, M. R., Zhang, Q., Jimenez, J. L., Tian, J., Ulbrich, I. M., Kroll, J. H., Docherty, K. S., Chhabra, P. S., Bahreini, R., Murphy, S. M., Seinfeld, J. H., Hildebrandt, L., Donahue, N. M., DeCarlo, P. F., Lanz, V. A., Prévôt, A. S. H., Dinar, E., Rudich, Y., and Worsnop, D. R.: Organic aerosol components observed in Northern Hemispheric datasets from Aerosol Mass Spectrometry, Atmos. Chem. Phys., 10, 4625–4641, doi:10.5194/acp-10-4625-2010, 2010.

Olszyna, K. J., Bailey, E. M., Simonaitis, R., and Meagher, J. F.: O_3 and NO_y relationships at a rural site, J. Geophys. Res.-Atmos., 99, 14557–14563, 1994.

Pandey Deolal, S., Brunner, D., Steinbacher, M., Weers, U., and Staehelin, J.: Long-term in situ measurements of NO_x and NO_y at Jungfraujoch 1998–2009: time series analysis and evaluation, Atmos. Chem. Phys., 12, 2551–2566, doi:10.5194/acp-12-2551-2012, 2012.

Parrish, D. D., Hahn, C. J., Williams, E. J., Norton, R. B., and Fehsenfeld, F. C.: Indications of photochemical histories of pacific air masses from measurements of atmospheric trace species at Point Arena, California, J. Geophys. Res.-Atmos., 97, 15883–15901, 1992.

Pochanart, P., Akimoto, H., Kinjo, Y., and Tanimoto, H.: Surface ozone at four remote island sites and the preliminary assessment of the exceedances of its critical level in Japan, Atmos. Environ., 36, 4235–4250, 2002.

Roberts, J. M., Fehsenfeld, F. C., Liu, S. C., Bollinger, M. J., Hahn, C., Albritton, D. L., and Sievers, R. E.: Measurements of aromatic hydrocarbon ratios and NO_x concentrations in the rural troposphere: observations of air mass photochemical aging and NO_x removal, Atmos. Environ., 18, 2414–2432, 1984.

Roussel, P. B., Lin, X., Camacho, F., Laszlo, S., Taylor, R., Melo, O., Shepson, P. B., Hastie, D., and Melo, O. T.: Observations of ozone and precursor levels at two sites around Toronto, Ontario, during SONTOS 92, Atmos. Environ., 30, 2145–2155, 1996.

Rudolph, J. and Johnen, F. J.: Measurements of light atmospheric hydrocarbons over the Atlantic in regions of low biological activity, J. Geophys. Res.-Atmos., 95, 20583–20591, 1990.

Sadanaga, Y., Fukumori, Y., Kobashi, T., Nagata, M., Takenaka, N., and Bandow, H.: Development of a selective light-emitting diode photolytic NO_2 converter for continuously measuring NO_2 in the atmosphere, Anal. Chem., 82, 9234–9239, 2010.

Seinfeld, J. H. and Pandis, S. N.: Atmospheric Chemistry and Physics, A Wiley Interscience Publication, New York, USA, 1997.

Suthawaree, J., Kato, S., Takami, A., Kadena, H., Toguchi, M., Yogi, K., Hatakeyama, S., and Kajii, Y.: Observation of ozone and carbon monoxide at Cape Hedo, Japan: seasonal variation and influence of long-range transport, Atmos. Environ., 42, 2971–2981, 2008.

Takami, A., Miyoshi, T., Shimono, A., and Hatakeyama, S.: Chemical composition of fine aerosol measured by AMS at Fukue Island, Japan during APEX period, Atmos. Environ., 39, 4913–4924, 2005.

Takami, A., Miyoshi, T., Shimono, A., Kaneyasu, N., Kato, S., Kajii, Y., and Hatakeyama, S.: Transport of anthropogenic aerosols from Asia and subsequent chemical transformation, J. Geophys. Res.-Atmos., 112, D22S31, doi:10.1029/2006JD008120, 2007.

Takegawa, N., Kondo, Y., Koike, M., Chen, G., Machida, T., Watai, T., Blake, D. R., Streets, D. G., Woo, J.-H., Carmichael, G. R., Kita, K., Miyazaki, Y., Shirai, T., Liley, J. B., and Ogawa, T.: Removal of NO_x and NO_y in Asian outflow plumes: aircraft measurements over the western Pacific in January 2002. J. Geophys. Res.-Atmos., 109, D23S04, doi:10.1029/2004JD004866, 2004.

Takegawa, N., Miyakawa, T., Kondo, Y., Blake, D. R., Kanaya, Y., Koike, M., Fukuda, M., Komazaki, Y., Miyazaki, Y., Shimono, A., and Takeuchi, T.: Evolution of submicron or-

ganic aerosol in polluted air exported from Tokyo, Geophys. Res. Lett., 33, L15814, doi:10.1029/2006GL025815, 2006.

Takiguchi, Y., Takami, A., Sadanaga, Y., Lun, X., Shimizu, A., Matsui, I., Sugimoto, N., Wang, W., Bandow, H., and Hatakeyama, S.: Transport and transformation of total reactive nitrogen over the East China Sea, J. Geophys. Res.-Atmos., 113, D10306, doi:10.1029/2007JD009462, 2008.

Tang, J. H., Chan, L. Y., Chang, C. C., Liu, S., and Li, Y. S.: Characteristics and sources of non-methane hydrocarbons in background atmospheres of eastern, southwestern, and southern China, J. Geophys. Res.-Atmos., 114, D033, doi:10.1029/2008JD010333, 2009.

Tanimoto, H., Sawa, Y., Yonemura, S., Yumimoto, K., Matsueda, H., Uno, I., Hayasaka, T., Mukai, H., Tohjima, Y., Tsuboi, K., and Zhang, L.: Diagnosing recent CO emissions and ozone evolution in East Asia using coordinated surface observations, adjoint inverse modeling, and MOPITT satellite data, Atmos. Chem. Phys., 8, 3867–3880, doi:10.5194/acp-8-3867-2008, 2008.

Ulbrich, I. M., Canagaratna, M. R., Zhang, Q., Worsnop, D. R., and Jimenez, J. L.: Interpretation of organic components from Positive Matrix Factorization of aerosol mass spectrometric data, Atmos. Chem. Phys., 9, 2891–2918, doi:10.5194/acp-9-2891-2009, 2009.

Yokouchi, Y.: Development of real-time monitoring system for non-methane hydrocarbons in the atmosphere, Final Report for Environmental Technology Development Fund, Ministry of the Environment, 2008 (in Japanese).

Yokouchi, Y., Takami, A., and Ohara, T.: Observational and modeling study of the high-ozone episode in northern Kyusyu focused on the impact of ozone precursors, Report of Special Research from the National Institute for Environmental Studies, Japan, 2011 (in Japanese).

Yuba, A., Sadanaga, Y., Takami, A., Hatakeyama, S., Takenaka, N., and Bandow, H.: Measurement system for particulate nitrate based on the scrubber difference $NO-O_3$ chemiluminescence method in remote areas, Anal. Chem., 82, 8916–8921, 2010.

Wang, M., Shao, M., Chen, W., Lu, S., Liu, Y., Yuan, B., Zhang, Q., Zhang, Q., Chang, C.-C., Wang, B., Zeng, L., Hu, M., Yang, Y., and Li, Y.: Trends of non-methane hydrocarbons (NMHC) emissions in Beijing during 2002–2013, Atmos. Chem. Phys., 15, 1489–1502, doi:10.5194/acp-15-1489-2015, 2015.

Zhang, Q., Worsnop, D. R., Canagaratna, M. R., and Jimenez, J. L.: Hydrocarbon-like and oxygenated organic aerosols in Pittsburgh: insights into sources and processes of organic aerosols, Atmos. Chem. Phys., 5, 3289–3311, doi:10.5194/acp-5-3289-2005, 2005.

Title Page

Abstract | Introduction

Conclusions | References

Tables | Figures

|◄ | ►|

◄ | ►

Back | Close

Full Screen / Esc

Printer-friendly Version

Interactive Discussion

Table 1. Concentrations and mixing ratios of chemical species observed during the study period.

	n	Mean	SD	Min[a]	Max	Lower quartile	Median	Upper quartile
Fine PM		($\mu g\,m^{-3}$)						
Chloride	22 726	0.08	0.12	LDL	2.65	0.03	0.04	0.09
Ammonium		1.5	1.6	LDL	14.7	0.59	1.05	1.8
Nitrate		0.69	1.43	LDL	22.00	0.12	0.25	0.63
Sulfate		4.2	3.3	LDL	23.8	2.0	3.4	5.5
Organics		2.7	1.9	LDL	24.5	1.4	2.2	3.4
Total[b]		9.2	7.4	0.02	66.7	4.7	7.5	11.2
m/z 43 in organics		0.18	0.14	LDL	4.17	0.08	0.14	0.22
m/z 44 in organics		0.40	0.30	0.06	2.45	0.20	0.33	0.50
m/z 57 in organics		0.03	0.04	0.01	1.87	0.02	0.03	0.04
Gas-phase species		(ppbv)						
CO	4163	230	102	57	1136	160	204	272
NO_x	4176	1.39	1.16	LDL	12.70	0.70	1.10	1.70
NO_y	4163	4.86	3.49	0.13	25.41	2.49	3.95	6.03
O_3	4165	45	11	10	97	38.3	44.8	52
i-Pentane	3856	0.11	0.08	LDL	2.05	0.07	0.10	0.13
Toluene	3856	0.11	0.14	LDL	2.63	0.04	0.07	0.12
Ethyne	3856	0.50	0.33	0.01	4.44	0.30	0.41	0.60

[a] LDL: lower than detection limit.
[b] Sum of chloride, ammonium, nitrate, sulfate, and organics.

Photochemical age and oxidation products in transboundary air, Japan

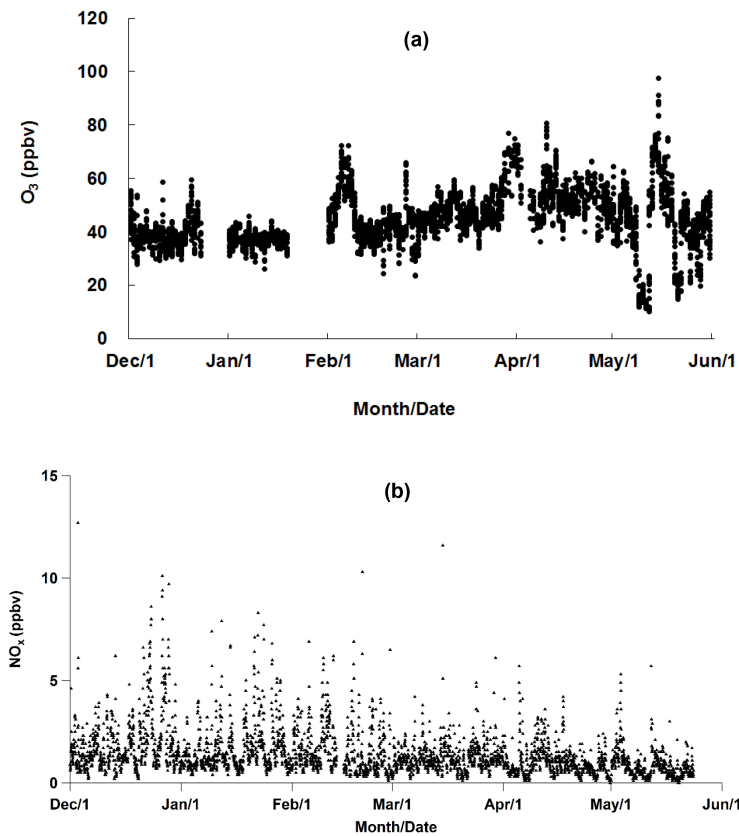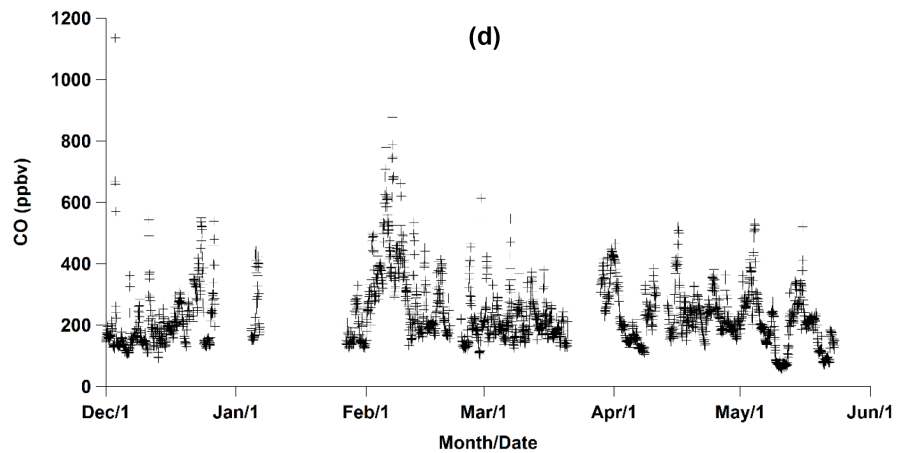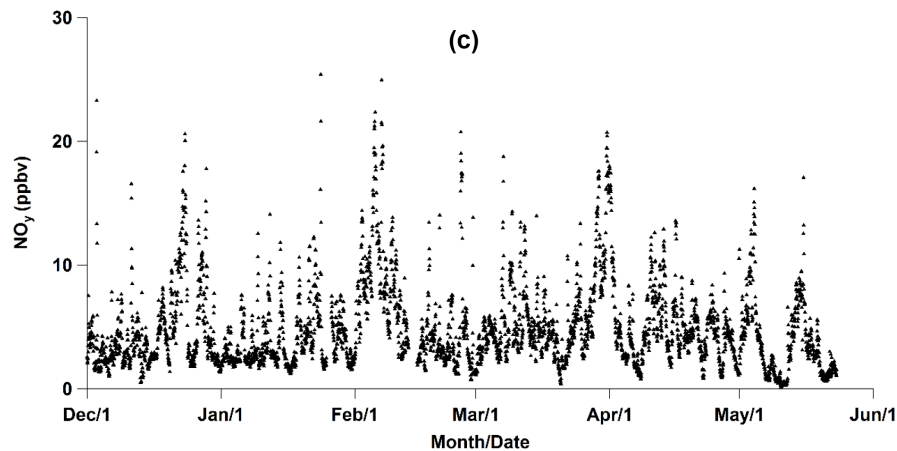S. Irei et al.

Title Page

Abstract | Introduction

Conclusions | References

Tables | Figures

|◀ | ▶|

◀ | ▶

Back | Close

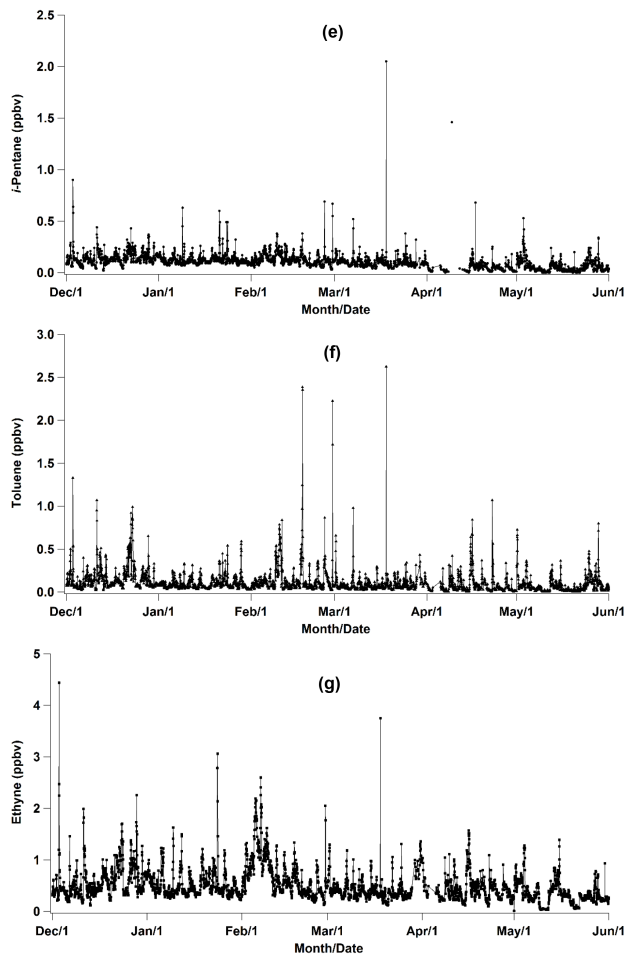Full Screen / Esc

Printer-friendly Version

Interactive Discussion

Table 2. Coefficients of determination for correlations between chemical species concentrations.

	PM_NH$_4$	PM_NO$_3$	PM_SO$_4$	PM_org	m/z 43	m/z 44	m/z 57	O$_3$	NO$_x$	NO$_y$	CO	i-Pentane	Toluene	Ethyne
PM_NH$_4$	1	0.693	0.639	0.696	0.443	0.755	0.323	0.251	0.007	0.480	0.405	0.004	0.026	0.097
PM_NO$_3$	0.693	1	0.263	0.529	0.389	0.521	0.320	0.145	0.035	0.544	0.314	0.025	0.051	0.107
PM_SO$_4$	0.639	0.263	1	0.430	0.380	0.463	0.191	0.128	0.001	0.179	0.371	0.013	0.006	0.125
PM_org	0.696	0.529	0.430	1	0.747	0.949	0.606	0.303	0.053	0.559	0.562	0.060	0.081	0.198
m/z 43	0.443	0.389	0.380	0.747	1	0.640	0.588	0.146	0.153	0.459	0.543	0.100	0.094	0.301
m/z 44	0.755	0.521	0.463	0.949	0.640	1	0.471	0.384	0.016	0.510	0.526	0.007	0.039	0.142
m/z 57	0.323	0.320	0.191	0.606	0.588	0.471	1	0.098	0.160	0.417	0.394	0.106	0.137	0.236
O$_3$	0.251	0.145	0.128	0.303	0.146	0.384	0.098	1	0.007	0.292	0.288	0.013	0.006	0.053
NO$_x$	0.007	0.035	0.001	0.053	0.153	0.016	0.160	0.007	1	0.309	0.136	0.195	0.225	0.221
NO$_y$	0.480	0.544	0.179	0.559	0.459	0.510	0.417	0.292	0.309	1	0.674	0.117	0.155	0.422
CO	0.405	0.314	0.371	0.562	0.543	0.526	0.394	0.288	0.136	0.674	1	0.193	0.126	0.724
i-Pentane	0.004	0.025	0.013	0.060	0.100	0.007	0.106	0.013	0.195	0.117	0.193	1	0.410	0.435
Toluene	0.026	0.051	0.006	0.081	0.094	0.039	0.137	0.006	0.225	0.155	0.126	0.410	1	0.302
Ethyne	0.097	0.107	0.125	0.198	0.301	0.142	0.236	0.053	0.221	0.422	0.724	0.435	0.302	1

Table 3. Three different combinations of model parameters.

Parameters	Combination I[a]	Combination II[a]	Combination III[b]
a ($\mu g\,C\,m^{-3}$)	0.05	0.0175	0.05
b ($\mu g\,C\,m^{-3}$)	1	1	1
$^{HOA}f_{44}$	0	0	0.08
$^{LV\text{-}OOA}f_{44}$	0.237	0.2371	0.22
$(OM/OC)_{HOA}$ ($\mu g\,\mu g\,C^{-1}$)	2.865	2.865	1.2
$(OM/OC)_{LV\text{-}OOA}$ ($\mu g\,\mu g\,C^{-1}$)	4.973	4.973	3.7

[a] The f_{44} and OM/OC values for HOA and LV-OOA are based on the results from the PMF analysis.
[b] Parameters used in the previous report (Irei et al., 2014, supportive information).
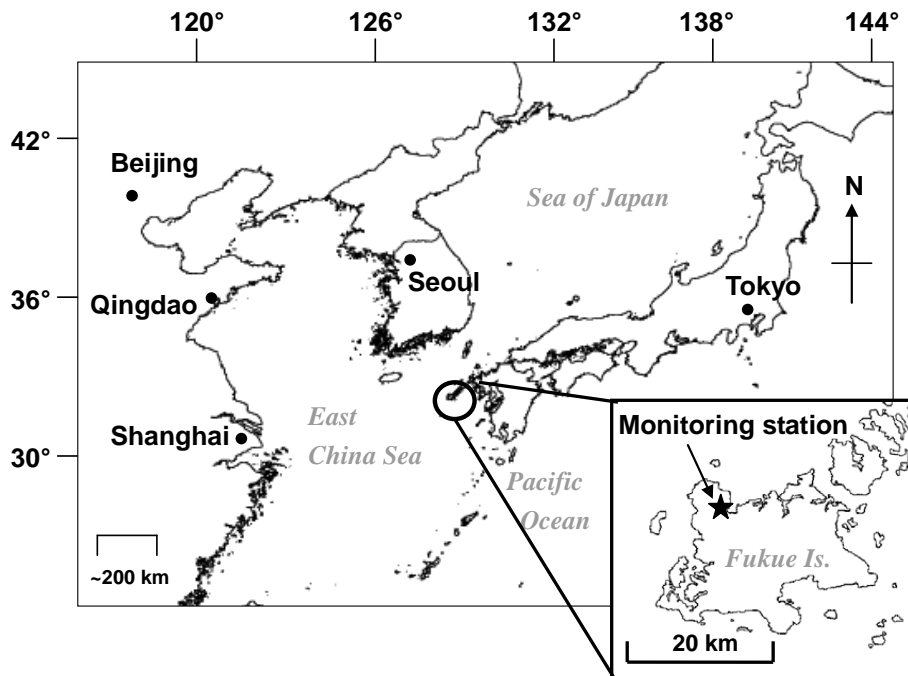
Figure 1. Location of the Fukue Island monitoring station.

Title Page

Abstract | Introduction

Conclusions | References

Tables | Figures

|◀ | ▶|

◀ | ▶

Back | Close

Full Screen / Esc

Printer-friendly Version

Interactive Discussion
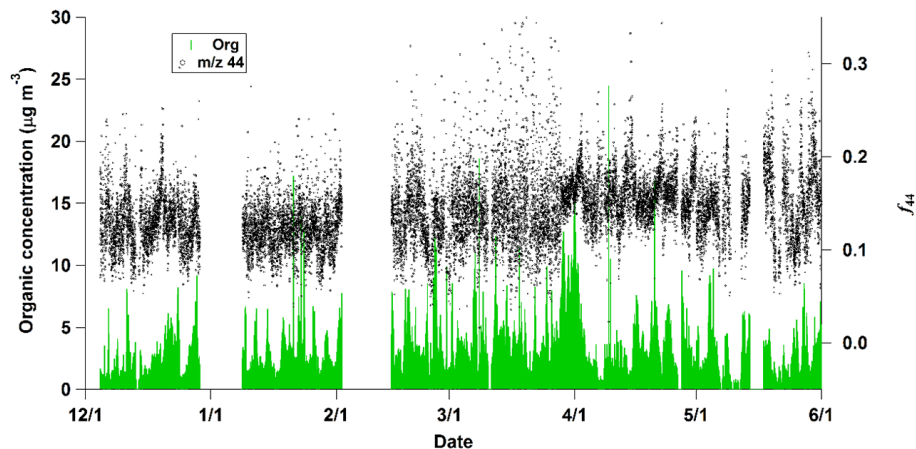
Figure 2. Temporal variation of concentration of organic species and fraction due to m/z 44, f_{44}, in the mass spectra of organic species measured by quadrupole aerosol mass spectrometry.

Title Page

Abstract | Introduction

Conclusions | References

Tables | Figures

|◄ | ►|

◄ | ►

Back | Close

Full Screen / Esc

Printer-friendly Version

Interactive Discussion

Figure 3.

Figure 3.

Figure 3. Temporal variation of hourly average mixing ratios for **(a)** O_3, **(b)** NO_x, **(c)** NO_y, **(d)** CO, **(e)** *i*-pentane, **(f)** toluene, and **(g)** ethyne.

Title Page

Abstract | Introduction

Conclusions | References

Tables | Figures

|◄ | ►|

◄ | ►

Back | Close

Full Screen / Esc

Printer-friendly Version

Interactive Discussion
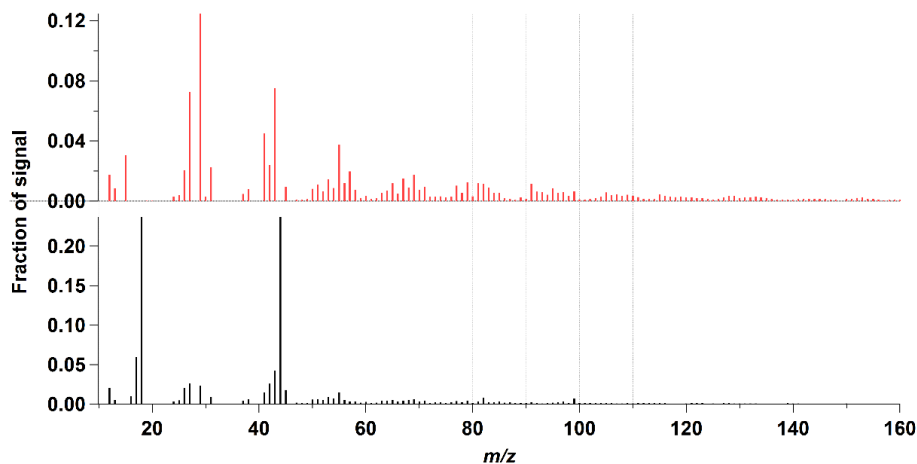
Figure 4. Extracted mass spectra from two-factorial PMF analysis: top, mass spectra identified as hydrocarbon-like organic aerosol (HOA, red); bottom, mass spectra identified as low-volatile oxygenated organic aerosol (LV-OOA, black).
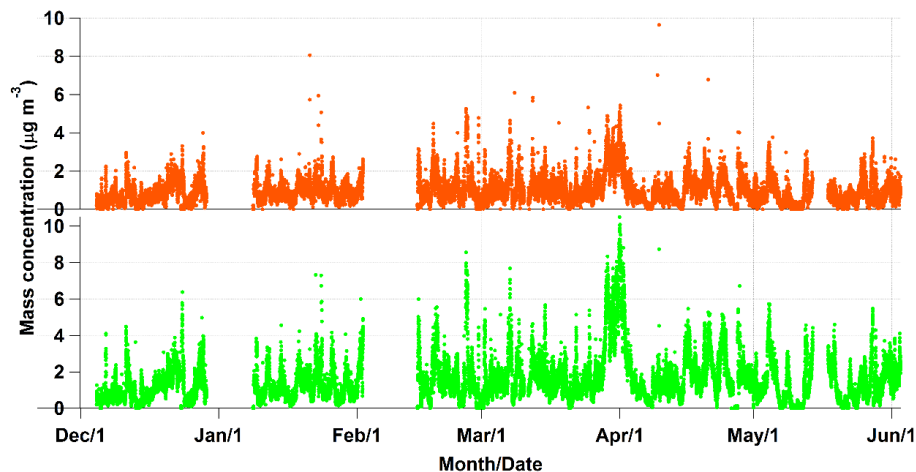
Figure 5. Temporal variation of mass concentration of HOA (orange) and LV-OOA (green) obtained by PMF analysis.
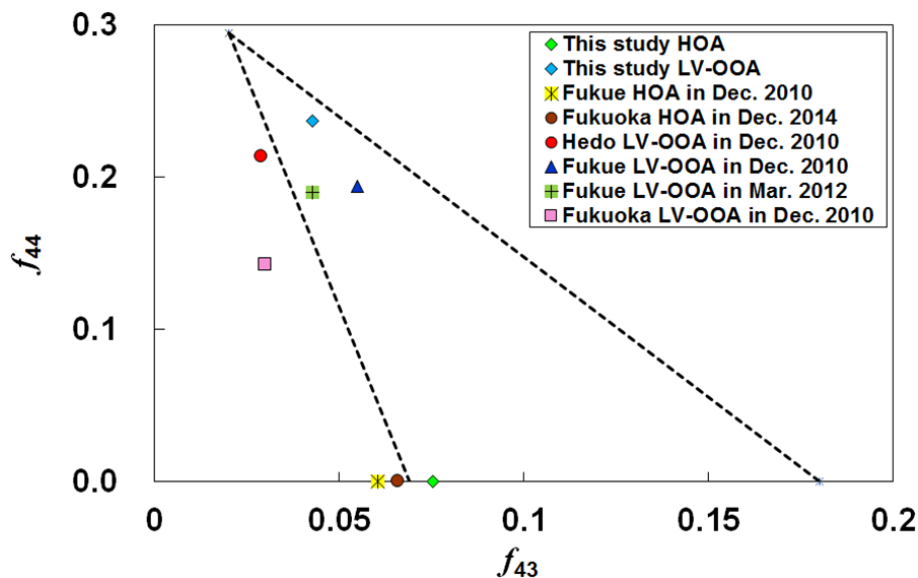
Figure 6. Plot of f_{44} vs. f_{43} for different types of organic aerosols extracted from PMF analysis. Dashed lines are the limits of oxidation states reported by Ng et al. (2010).
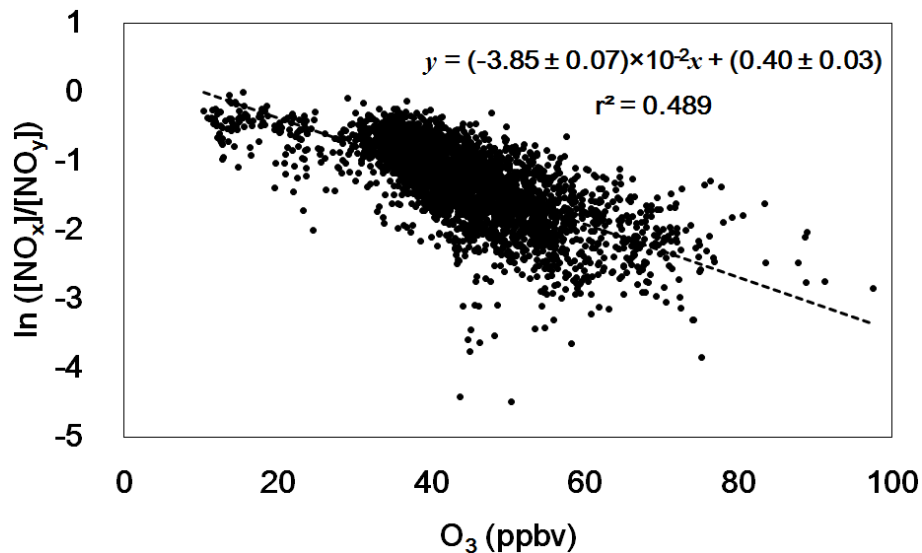
Figure 7. Scatter plot of natural logarithm of $[NO_x]/[NO_y]$ ratio vs. O_3 mixing ratio.
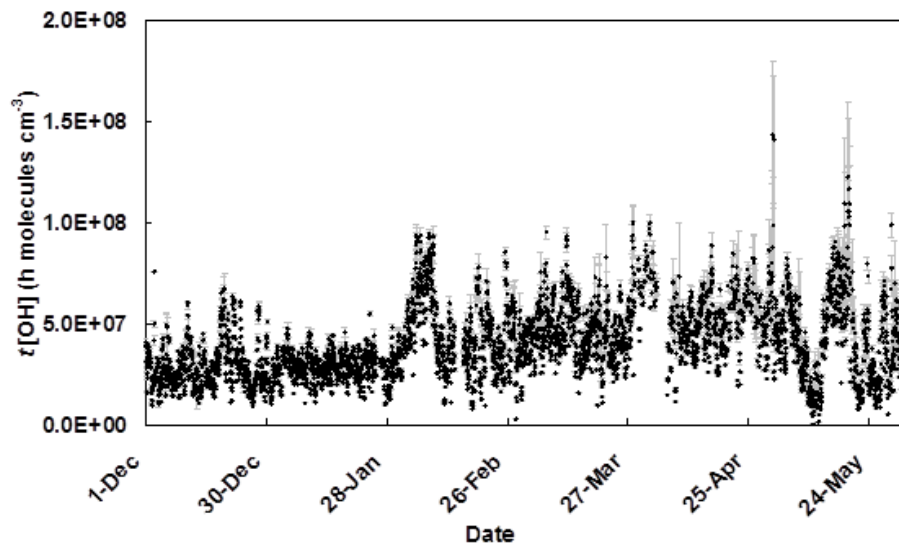
Figure 8. Time-series variation of photochemical age, t[OH], estimated from $[NO_x]/[NO_y]$ ratios. Error bars shown are estimated standard errors based on the uncertainties of NO_x and NO_y measurements.
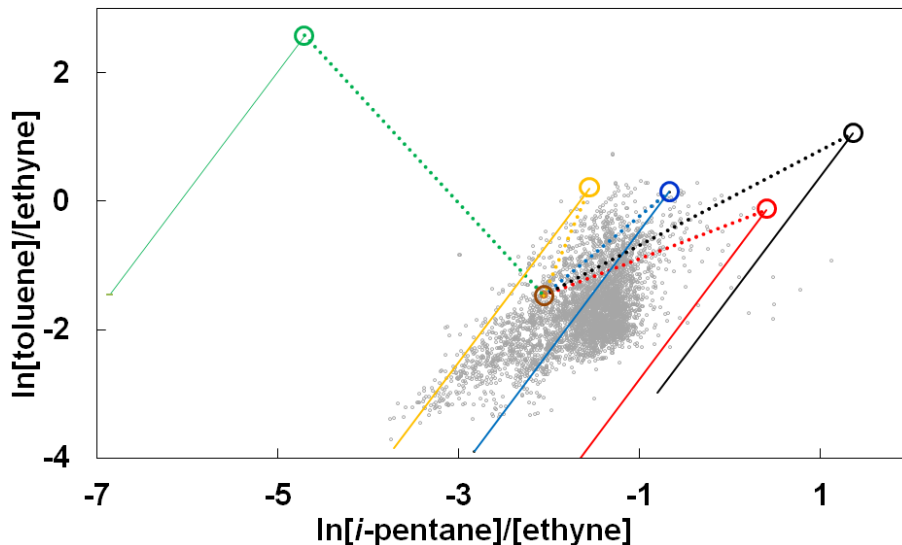
Figure 9. Scatter plot of natural logarithm of [toluene]/[ethyne] ratio as function of natural logarithm of [*i*-pentane]/[ethyne] ratio (gray dots). Linear regressions shown are calculated depletion trends resulting from mixing with background air (dotted lines) and from reaction with OH radicals (solid lines); these trends were determined by using the initial NMHC ratios from the literature, for vehicular emissions 1 (black open circle), vehicular emissions 2 (red open circle), solvent use (green open circle), and natural gas and gasoline leakage (blue open circle) observed in Beijing (Wang et al., 2015), as well as field measurement data obtained at Lin'an, a rural background site in the Yangtze River Delta, China (yellow open circle) from Tang et al. (2009). The brown open circle that all the dotted lines meet at corresponds to the background values observed at Cape Hedo (Kato et al., 2004). See the text for the calculation and references for these data.

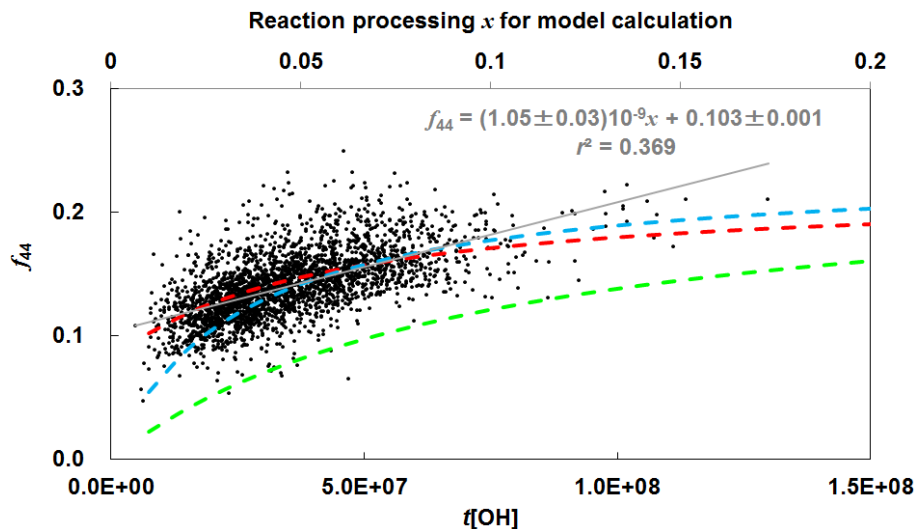**Figure 10.** Scatter plot of hourly averaged f_{44} (black dot) as function of photochemical age, $t[OH]$, estimated by means of the NO_x/NO_y clock (the bottom x axis) and a linear regression (grey line). As comparison, f_{44} binary mixing models (dotted curves) of HOA and LV-OOA using different combinations of model parameters (combination I (green); combination II (blue); and combination III (red)) are also shown. See the text for the detail of the combinations of model parameters.

Title Page

Abstract | Introduction

Conclusions | References

Tables | Figures

|◄ | ►|

◄ | ►

Back | Close

Full Screen / Esc

Printer-friendly Version

Interactive Discussion